to 1 part in 10,[4] the hyperfine anomalies (as defined on p. 280 of Ref.6) can be calculated. The results are given in Table V. The precision is, at present, limited by the uncertainties given for the ratios of the dipole moments.

The magnetic field produced at the Sn nucleus by the electronic configuration can be obtained from the relation[2]

$$H_J=-\frac{haIJ}{\mu_I}. \tag{6}$$

From Tables II and IV and Eq. (6), the internal fields are found to be

$$H(^3P_1)=+0.3626\times10^6\ \mathrm{G},$$
$$H(^3P_2)=-1.592\times10^6\ \mathrm{G},$$

to within about 0.1%.

ACKNOWLEDGMENTS

The authors would like to thank B. Budick for a helpful private communication. They are extremely grateful to Brian Wybourne for extensive hfs calculations and numerous helpful discussions.

PHYSICAL REVIEW VOLUME 137, NUMBER 1A 4 JANUARY 1965

Approximate Methods for Obtaining Radial Distribution Functions of Fluids*

D. D. CARLEY AND F. LADO
Department of Physics, University of Florida, Gainesville, Florida
(Received 14 August 1964)

Two integral equations are proposed whose solutions approximate the radial distribution function of classical fluids whose single-component particles interact with pairwise radial forces. Solutions to these equations are obtained for several temperature and density conditions for particles interacting with potentials corresponding to the Lennard-Jones, the hard-sphere, and the Gaussian models. When Monte Carlo results are used as a standard, these new equations provide answers which often show improvement over the answers obtained by the Percus-Yevick or convolution-hypernetted-chain equations.

I. INTRODUCTION

THE theory of fluids in thermodynamic equilibrium has undergone considerable progress in recent years as a result of studies of the radial distribution function g[1]. Although several new methods have been advanced for computing g, the convolution-hypernetted-chain[2] (CHNC) and the Percus-Yevick[3] (PY) equations have received the greatest attention. A large number of solutions have now been obtained for these equations over a wide range of temperature and density conditions for several forms of the pair potential function[4] and these results indicate that the PY and CHNC equations provide considerable improvement over previous methods. However, neither the PY nor the CHNC equation has obtained a clear advantage over the other for all potentials under varying temperature and density conditions.

The PY and CHNC equations may be looked upon as a partial summation of terms[5] (from all orders of density) of the density expansion for g. The CHNC summation includes all the terms summed by PY plus an additional infinite set. The remarkable success of the PY equation, in spite of its summation of fewer terms, suggests that there is often better cancellation among the terms omitted than in the CHNC equation. The techniques of summation of certain terms from the density expansion, as exemplified by the CHNC and PY equations, suggests two possible procedures for obtaining better distribution functions: (1) to systematically include more terms in the summation or (2) to eliminate more terms or to weight certain ones differently to obtain better cancellation among the terms

* This research was supported in part by the National Science Foundation and the National Aeronautics and Space Administration.

[1] For a general discussion of the radial distribution function, its relationship to various thermodynamic quantities, and its role in the theory of fluids, see, J. O. Hirschfelder, C. F. Curtiss, and R. B. Bird, *Molecular Theory of Gases and Liquids* (John Wiley & Sons, Inc., New York, 1954).

[2] E. Meeron, J. Math. Phys. **1**, 192 (1960); T. Morita, Progr. Theoret. Phys. (Kyoto) **23**, 385 (1960); J. M. J. Van Leeuwen, J. Groeneveld, and J. DeBoer, Physica **25**, 792 (1959); M. S. Green, Technical Report, Hughes Aircraft Corporation (unpublished).

[3] J. K. Percus and G. J. Yevick, Phys. Rev. **110**, 1 (1958); J. K. Percus, Phys. Rev. Letters **8**, 462 (1962).

[4] A. A. Broyles, J. Chem. Phys. **33**, 456 (1960); **34**, 359, 1068 (1961); **35**, 493 (1961); A. A. Broyles, S. U. Chung, and H. L. Sahlin, *ibid.* **37**, 2462 (1962); A. A. Khan, Phys. Rev. **134**, A367 (1964); D. D. Carley, *ibid.* **131**, 1406 (1963); D. D. Carley, *ibid.* **136**, A127 (1964); M. Klein, J. Chem. Phys. **39**, 1388 (1963); M. Klein and M. S. Green, *ibid.* **39**, 1367 (1963); M. Klein, Phys. Fluids **7**, 391 (1963); M. S. Wertheim, Phys. Rev. Letters **10**, 321 (1963).

[5] The original derivation as published by Percus and Yevick employed collective coordinates. G. Stell studied the equation from the summation point of view. G. Stell, Physica **29**, 517 (1963). See also Khan, Ref. 4.

omitted.[6] An important consideration must be the time or effort involved in making these corrections since if the method is too laborious or involved the time might be better spent in obtaining Monte Carlo[7] (MC) solutions. It is in the spirit of (2) that in this paper we present two equations for obtaining radial distribution functions and apply them to the Lennard-Jones, the hard-sphere, and the Gaussian models. We compare these calculations with results obtained by Monte Carlo methods which we take as a standard. The main advantages of the integral-equation methods over the Monte Carlo method are the greatly reduced computer time needed to obtain solutions and the possibility of solving the integral equations for the potential when given an experimental g.

II. SUMMARY OF SOME WELL-KNOWN RESULTS

We are concerned with a classical one-component fluid having an average number density

$$\bar{n}=N/V, \tag{1}$$

where N is the number of particles and V is the volume. The potential energy U of the system is assumed to be the sum of pair potentials so that

$$U(\mathbf{r}_1,\cdots\mathbf{r}_N)=\tfrac{1}{2}\sum_{i,j=1,i\neq j}^{N}\phi(r_{ij}), \tag{2}$$

where r_{ij} is the separation between particles i and j. For a system in equilibrium at temperature T, the radial distribution function is given by[1]

$$g(r_{12})=V^2Z^{-1}\int_V\cdots\int e^{-\beta U}d\mathbf{r}_3\cdots d\mathbf{r}_N, \tag{3}$$

where

$$Z=\int_V\cdots\int e^{-\beta U}d\mathbf{r}_1\cdots d\mathbf{r}_N \tag{4}$$

and

$$\beta=(kT)^{-1}. \tag{5}$$

Equation (3) is valid in the limit of $N\to\infty$, $V\to\infty$, and $\bar{n}$ remaining constant. Boltzmann's constant is denoted by k.

Thermodynamic quantities can be calculated from the radial distribution function. In particular, the mean potential energy $\bar{U}$ is given by

$$E\equiv\beta\bar{U}/N=2\pi\bar{n}\beta\int_0^\infty\phi(r)g(r)r^2dr, \tag{6}$$

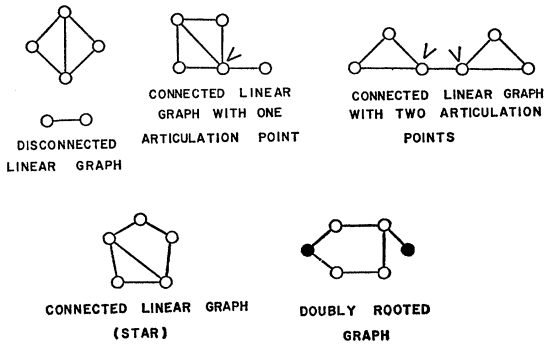

FIG. 1. Examples of the nomenclature of linear graphs.

and the pressure p by

$$P^*\equiv p\beta/\bar{n}=1-\frac{2\pi\bar{n}\beta}{3}\int_0^\infty\frac{d\phi(r)}{dr}g(r)r^3dr. \tag{7}$$

The isothermal compressibility K, in terms of the correlation function G, is given by

$$K=-\frac{1}{V}\left(\frac{\partial V}{\partial p}\right)_T=\beta\left[\bar{n}^{-1}+4\pi\int_0^\infty r^2G(r)dr\right], \tag{8}$$

where

$$G(r)\equiv g(r)-1. \tag{9}$$

The radial distribution function can be written as a power series in density.[8] This expansion is best described in terms of linear graphs or diagrams.

A *linear graph* is a collection of points with lines joining certain pairs of points.[9] The graph is *disconnected* if it is composed of two or more groups having no line joining a point of one group with a point of the other. If a graph is not disconnected it is *connected*. A point is an *articulation point* of a connected graph if, when it is removed, the graph becomes disconnected. A connected graph which contains no articulation points is a *star*. A graph is a *rooted* graph if one point or a subset of points of the graph has been given a special designation. In the study of radial distribution functions, *doubly-rooted* graphs are of importance. Figure 1 illustrates some of these definitions.

There is associated with each connected linear graph products of Mayer f functions,

$$f(r_{ij})=\exp[-\beta\phi(r_{ij})]-1, \tag{10}$$

such that there is a correspondence between the linear graphs and integrals over products of f functions. It is convenient to associate integration over the coordinates of the particles with the nonroot (or field) points. We

[6] L. Verlet and D. Levesque, Physica **28**, 1124 (1962); M. Klein, Phys. Fluids **7**, 391 (1963); G. S. Rushbrooke and P. Hutchinson, Physica **27**, 647 (1961); P. Hutchinson and G. S. Rushbrooke, *ibid.* **29**, 675 (1963).

[7] For a discussion of the Monte Carlo method, see, N. Metropolis, A. W. Rosenbluth, M. N. Rosenbluth, A. H. Teller, and E. Teller, J. Chem. Phys. **21**, 1087 (1953); W. W. Wood and T. R. Parker, *ibid.* **27**, 720 (1957).

[8] J. E. Mayer and E. W. Montroll, J. Chem. Phys. **9**, 626 (1941).

[9] There seems to be a great diversity in the current literature in the notation used to describe the diagrammatic methods. Here we follow quite closely Uhlenbeck and Ford. For more details concerning the following paragraphs, see J. DeBoer and G. E. Uhlenbeck, *Studies in Statistical Mechanics* (North-Holland Publishing Company, Amsterdam, 1962).

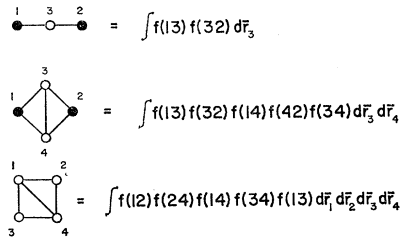

FIG. 2. Examples of the correspondence between diagrams and integrals of Mayer f functions.

will denote the field points by open circles and the rooted points by black circles. Figure 2 illustrates the correspondence between the diagrams and integrals. A line between points i and j denotes the presence of the factor $f(ij)$ in the corresponding integral.[10]

The radial distribution function as a power series in density can now be written as

$$ge^{\beta\phi}=1+\sum_{k=3}^{\infty}\frac{\bar{n}^{(k-2)}}{(k-2)!}\int\cdots\int\Big(\sum_{(Q_k)}\prod_{Q_k}f_{ij}\Big)d\mathbf{r}_3\cdots d\mathbf{r}_k, \quad (11)$$

where the integrals over the sum of products of f functions are those corresponding to all doubly-rooted graphs Q_k of k labeled points, which become stars when points 1 and 2 are connected. [Points 1 and 2 are the rooted points and are not connected in the diagrams of Eq. (11).] This expansion through $\bar{n}^2$ is given in Fig. 3.

It is convenient to classify the diagrams Q_k described above into series, parallel, and bridge diagrams. If all paths from 1 to 2 pass through a given point, the point is a *nodal point*. A diagram which contains one or more nodal points is a *series* diagram. If the graph

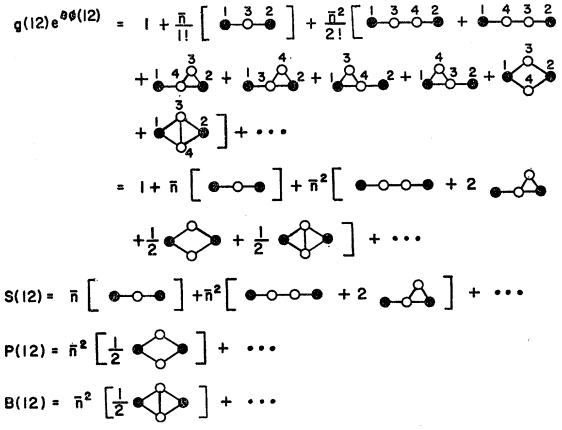

FIG. 3. The density expansions for $g\exp(\beta\phi)$, S, P, and B through $\bar{n}^2$. In the top equation the points are labeled according to Eq. (11). Because the values of the diagrams do not depend upon the labels of the field points and because the functions of 1 and 2 are symmetric, many of the terms may be combined, as in the other equations in this figure.

[10] For ease in writing we will often use the shorter notation $f(ij)$ for $f(r_{ij})$, $\phi(ij)$ for $\phi(r_{ij})$, etc.

breaks into two or more disconnected graphs when points 1 and 2 are removed, the diagram is a *parallel* diagram. If a diagram Q_k is neither a parallel nor a series diagram, then it is a *bridge* diagram. If we denote[11] the contribution to $g\exp(\beta\phi)$ in Eq. (11) of all series diagrams by $S(12)$, of all parallel diagrams by $P(12)$, and of all bridge diagrams by $B(12)$, Eq. (11) can be rewritten as

$$g(12)e^{\beta\phi(12)}=1+S(12)+P(12)+B(12). \quad (12)$$

Figure 3 lists the terms in $S(12)$, $P(12)$, and $B(12)$ through $\bar{n}$.[2]

Several useful relationships between these functions have been obtained and we list them here. First we

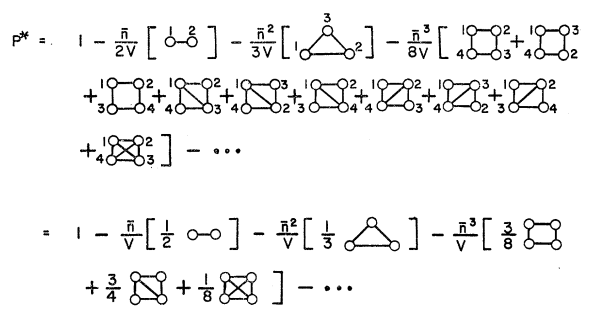

FIG. 4. The virial expansion for the pressure. In the top equation the diagrams have been labeled according to Eq. (17). Because the value of a given type of diagram does not depend upon the labels of the points, several terms may be combined as in the second equation.

define the direct correlation function T,

$$T(12)=G(12)-S(12). \quad (13)$$

It has been shown that[12]

$$P(12)=\exp[B(12)+S(12)]-1-S(12)-B(12) \quad (14)$$

and

$$G(12)=T(12)+\bar{n}\int G(13)T(32)d\mathbf{r}_3. \quad (15)$$

Finally, we will need the well known virial expansion for the pressure[1]

$$P^*=p\beta/\bar{n}=1+\sum_{j=2}^{\infty}B_j(T)\bar{n}^{(j-1)}, \quad (16)$$

where

$$B_j=-\frac{j-1}{j!V}\int\cdots\int\Big(\sum_{(S_j^*)}\prod_{S_j^*}f_{ij}\Big)d\mathbf{r}_1\cdots d\mathbf{r}_j. \quad (17)$$

These integrals of the sums of products of f functions correspond to all stars S_j^* with j labeled points. The expansion through $\bar{n}^3$ is listed in Fig. 4.

The virial expansion for the pressure is usually obtained without the use of the radial distribution

[11] This notation follows that of Klein and Green, Ref. 4.

[12] See, for example, Van Leeuwen *et al.*, Ref. 2.

function. However, it can be shown that Eqs. (16) and (17) can be obtained using the density expansion for g, Eq. (11) with either the pressure equation, Eq. (7), or the compressibility equation, Eq. (8).[13] For an approximate equation for g which sums only certain diagrams from the density expansion, corresponding virial expansions for the pressure can be obtained using either the pressure or compressibility equation, but the virial coefficients thus obtained will in general not be the same.

III. THE INTEGRAL EQUATIONS

Integral equations such as PY and CHNC are equivalent to partial summations of diagrams from the density expansion for $g\exp(\beta\phi)$. The diagrams summed by these equations are shown in Fig. 5 for diagrams through two field points and may be compared with the exact expansion in Fig. 3. The virial expansion for the pressure can be obtained from the compressibility equation for the PY and CHNC equations. This result is shown in Fig. 6.

It is seen that the PY and CHNC density expansion for $g\exp(\beta\phi)$ are exact only through one field point. As the number of field points increases, the number of diagrams neglected by these approximations increases rapidly.[14] From these considerations alone, it is clear only that the equations should be valid for low density where contributions from the individual neglected diagrams are small; however, numerical solutions indicate that these equations are good representations for densities much greater than this. Thus there must be cancellation among the neglected diagrams.

Since the cancellation is so important to the integral equation of the PY or CHNC type, and since these equations neglect a large number of diagrams, the possibility of obtaining better equations through better cancellation becomes quite appealing. Once the notion of summing more graphs is abandoned for the idea of selecting graphs, the number of interesting integral

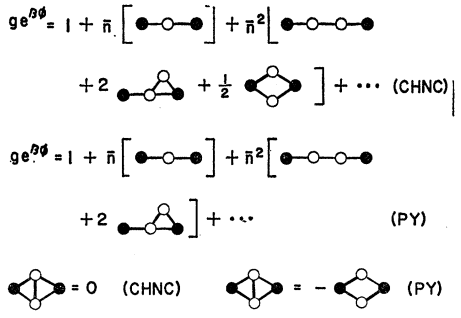

FIG. 5. The density expansions for $g\exp(\beta\phi)$ according to the PY and CHNC approximations. The last two equations are the approximations of diagrams through two field points.

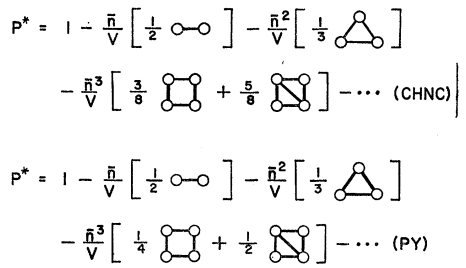

FIG. 6. The virial expansion for the pressure according to the PY and CHNC approximations as obtained from the compressibility equation.

equations for g becomes quite large. Here we limit ourselves to the study of two of these possibilities. Both of the equations displayed below contain a parameter which is determined by the particular temperature and type of potential of the system being studied. This parameter, which appears in diagrams of two or more field points, thus has the effect of allowing the conditions of the problem to adjust the approximation made, rather than fixing it beforehand, as in the PY and CHNC equations.

Equation (A)

From Eqs. (12), (13), (14), and (15), the following equations can be easily obtained:

$$g(12)e^{\beta\phi(12)}-1=P(12)+B(12)+\bar{n}\int G(13)[B(32)+P(32)+f(32)g(32)e^{\beta\phi(32)}]d\mathbf{r}_3, \quad (18)$$

$$P(12)=g(12)e^{\beta\phi(12)}-1-\ln[g(12)e^{\beta\phi(12)}]. \quad (19)$$

Equations (18) and (19) are still exact but the presence of the unknown set B prevents the formation of a closed set of equations for g. Equation (A) is obtained by making the approximation

$$B(12)\approx mP(12) \quad (20)$$

in Eq. (18).

Equation (A) can now be written as

$$g_A(12)e^{\beta\phi(12)}-1=(1+m)P_A(12)+\bar{n}\int G_A(13)[(1+m)P_A(32)+f(32)g_A(32)e^{\beta\phi(32)}]d\mathbf{r}_3, \quad (21)$$

$$P_A(12)=g_A(12)e^{\beta\phi(12)}-1-\ln[g_A(12)e^{\beta\phi(12)}]. \quad (22)$$

The parameter m is still to be chosen and later we will suggest a method for determining it. Note that the choice of m equal to 0 or -1 gives the CHNC and PY equations, respectively.

[13] J. DeBoer, Rept. Progr. Phys. 12, 305 (1949).
[14] E. Helfand and R. L. Kornegay, Physica (to be published).

Equation (B)

The equation

$$g(12)e^{\beta\phi(12)}=1+\bar{n}\int G(13)T(32)d\mathbf{r}_3 +a\left[\bar{n}\int G(13)T(32)d\mathbf{r}_3\right]^2 \quad (23)$$

contains the one-field-point diagram correctly, provided that T is given by

$$T(12)=f(12), \quad (24)$$

when g satisfies the equation

$$g(12)e^{\beta\phi(12)}=1. \quad (25)$$

Furthermore, the parameter a appears in more complex diagrams.[15] We also require G and T to satisfy the Ornstein-Zernicke relationship of Eq. (15). By combining Eqs. (15) and (23), we obtain

$$T(12)=G(12)+(2a)^{-1}\pm\tfrac{1}{2}\{a^{-2}-4a^{-1} \times[1-g(12)e^{\beta\phi(12)}]\}^{1/2}. \quad (26)$$

The sign before the radical is chosen so as to satisfy the condition of Eqs. (24) and (25). Equations (15) and (26) form Eq. (B). The density expansion for $g\exp(\beta\phi)$ can be obtained by iteration of Eq. (B), and the results through two field points are given in Fig. 7. Using this density expansion for $g\exp(\beta\phi)$, the corresponding pressure series may be obtained from the compressibility equation and this result is given in Fig. 8.

Determination of the Parameters

Equations (A) and (B) have been constructed so as to give the correct diagrams in the density expansion for $g\exp(\beta\phi)$ for terms with fewer than two field points (as is the case with PY and CHNC), thus insuring good results for low densities. In addition these equations contain a parameter, as yet unspecified, which appears

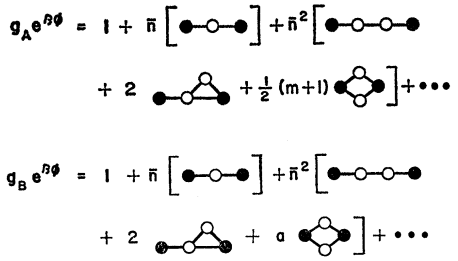

FIG. 7. The density expansion for $g\exp(\beta\phi)$ for Eqs. (A) and (B). Although the diagrams included through two field points can be made the same by the proper choice of a and m, the diagrams of greater complexity are quite different.

[15] We note that when a is taken to be $\frac{1}{2}$, Eq. (B) is similar in appearance to Klein's Eq. (13a) of Ref. 6. However, in terms of the diagrams summed, these two equations are quite different. Equation (B) is not a member of the sequence considered by Klein.

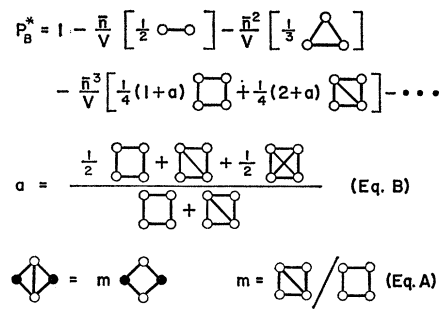

FIG. 8. The determination of the constants a and m. The first equation is the virial expansion for the pressure from Eq. (B) using the compressibility equation. Note that when $a=0$ the terms are the same as PY (Fig. 6), and when $a=\frac{1}{2}$ they are the same as CHNC. This is no longer true when more complex graphs are included. When a is chosen according to the second equation, the fourth virial coefficient is given correctly. The third equation shows the approximation in the expansion for $g\exp(\beta\phi)$ for Eq. A in the diagrams of two field points. In the last equation the method used for determining m is shown.

in the terms of two or more field points. The problem now is to select these parameters so as to obtain good results at higher densities. In choosing these parameters we were guided by the studies of the virial coefficients for the hard-sphere gas, made by Rushbrooke and Hutchinson.[6]

In the case of Eq. (B), the parameter a was chosen so as to obtain the correct fourth virial coefficient (as obtained from the compressibility equation). The equation for a in terms of diagrams is shown in Fig. 8.

For Eq. (A), the parameter m was chosen to approximate diagrams with two field points in the $g\exp(\beta\phi)$ expansion. If m were obtained by the third equation in Fig. 8, Eq. (A) would be correct through two field points. As an approximation to this, m has been chosen as in the fourth equation, making use of the virial diagrams. Thus m is in some sense an average value of f, and will depend on the pair potential chosen and the temperature of the system. The determination of m is somewhat easier than a since the double cross-bond diagram (see Fig. 8) is not present; this diagram is usually more difficult to evaluate than the other four-point stars.

It is not clear that the better representation of the fourth virial coefficient [in Eq. (B)] or the two-field-point diagram [in Eq. (A)] will necessarily result in improved results at high densities. The justification of these approximations ultimately must come from the ability of these equations to produce answers in good agreement with standard theoretical calculations (such as MC) or with experiment. We have, therefore, obtained solutions to these integral equations for certain potentials where standard results are available for comparison.

IV. NUMERICAL RESULTS

We have obtained numerical solutions to Eqs. (A) and (B) under selected conditions for the Lennard-

Jones, the hard-sphere, and the Gaussian models. These solutions are compared with Monte Carlo, PY, and CHNC results. The form of Eqs. (A) and (B) is similar to that of the PY and CHNC equations, so that the methods of solving the latter equations (see the references listed under Ref. 4) apply here also.

Gaussian Model

For the Gaussian model the Mayer f function is a negative Gaussian

$$f(r)=-\exp[-(r/\alpha)^2]. \tag{27}$$

We take 1.10 α as our unit of length[16] and define a reduced length x and density $\bar{n}^*$ according to the equations

$$x=r/(1.10\alpha) \tag{28}$$

and

$$\bar{n}^*=\bar{n}(1.10\alpha)^3. \tag{29}$$

Also, we define

$$C=\tfrac{1}{2}(\pi)^{3/2}\alpha^3. \tag{30}$$

The values of the integrals needed to determine a and

DIAGRAM	GAUSSIAN	HARD SPHERE	LENNARD-JONES ($T^*=2.74$)
$\frac{1}{V}$ 	1.00000 C^3	2.5905 D^3	9.32 σ^9
$\frac{1}{V}$ 	− 0.35355 C^3	− 1.8890 D^3	−6.82 σ^9
$\frac{1}{V}$ 	0.12500 C^3	1.267 D^3	4.70 σ^9

FIG. 9. Values of the virial diagrams needed in the determination of a and m.

m can be analytically evaluated[17] for the Gaussian model and are listed in Fig. 9. Thus we get

$$a=0.3232 \tag{31}$$

and

$$m=-0.3535. \tag{32}$$

Using these values the integral equations were solved for densities of $\bar{n}^*=0.35$ and $\bar{n}=1.00$ and compared with previous calculations for $g(x)$ using the PY, CHNC, and MC methods.[18] The results are shown in Figs. 10 and 11. At $\bar{n}^*=0.35$ there is excellent agreement between the MC, PY, CHNC, E5,[19] (A), and (B) results. For $\bar{n}^*=1.00$ there is close agreement between MC, CHNC, (A), and (B) with PY somewhat below the other curves.

[16] More precisely the unit of length is $(3\pi^{1/2}/4)^{1/3}\alpha$, as in Ref. 14.
[17] See Ref. 9.
[18] The PY, CHNC, and MC solutions are from D. D. Carley, Phys. Rev. 136, A127 (1964).
[19] E5 represents the radial distribution function as determined from an evaluation of all diagrams in the density expansion for $g\exp(\beta\phi)$ through the fifth power in density. At $\bar{n}^*=0.35$ this should give an excellent representation of g. This data is taken from Ref. 14.

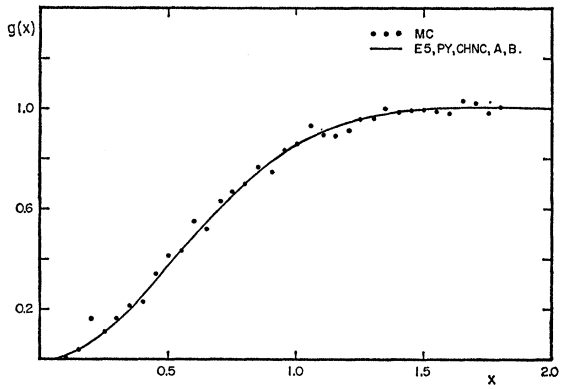

FIG. 10. Radial distribution functions for the Gaussian model for $\bar{n}^*=0.35$.

Hard Sphere

For the hard-sphere model the Mayer function is given by

$$f(r)=-1, \quad r<d \tag{33}$$

$$f(r)=0, \quad r>d \tag{34}$$

where d is the diameter of the hard sphere. Taking d as our unit of length we define

$$x=r/d, \tag{35}$$

$$\bar{n}^*=\bar{n}d^3, \tag{36}$$

and

$$D\equiv 2\pi d^3/3. \tag{37}$$

The values of the integrals necessary to determine a and m have been computed[20] and are listed in Fig. 9. From this table the constants are found to be

$$a=0.0567 \tag{38}$$

and

$$m=-0.7292. \tag{39}$$

Using these values the integral equations were solved for several densities and P^* was calculated using Eq.

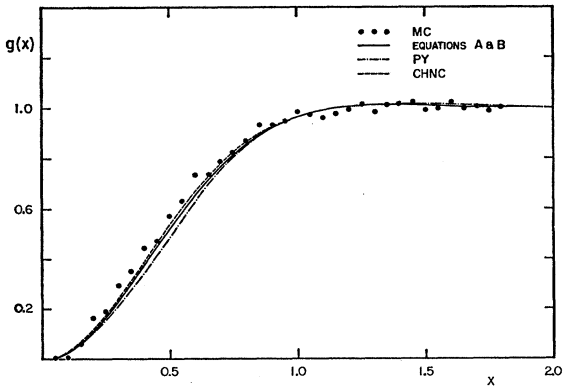

FIG. 11. Radial distribution functions for the Gaussian model for $\bar{n}^*=1.00$.

[20] See Ref. 9 and also references listed there.

(7). Figure 12 compares the $P^*(\bar{n}^*)$ reference isotherm used by Klein,[21] the PY, CHNC, (A), and (B) isotherms. We have also plotted $g(x)$ for $\bar{n}^*=0.789$ in Fig. 13. Both Eqs. (A) and (B) give results in much closer agreement with the reference isotherm than does the CHNC equation. The comparison of Eqs. (A) and (B) with PY is favorable, but the differences are quite small and a definite conclusion as to which is best is rather difficult. The problem is further complicated by the sensitivity of the hard-sphere solutions to the interval chosen for the numerical integrations.

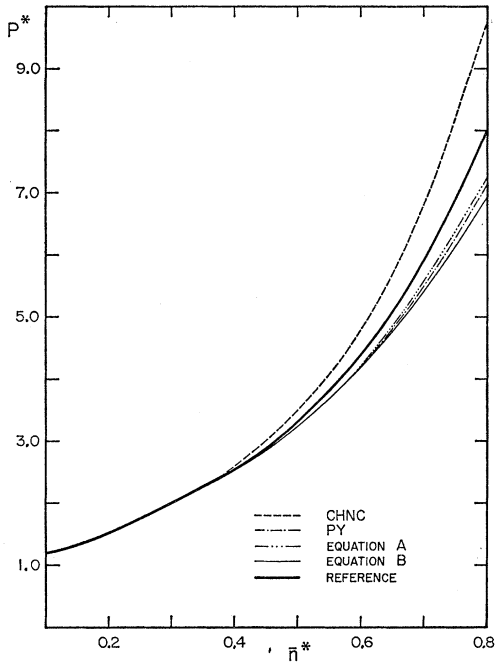

FIG. 12. Equations of state for hard spheres.

Lennard-Jones

The Lennard-Jones potential is given by

$$\phi(r)=4\epsilon[(\sigma/r)^{12}-(\sigma/r)^{6}]. \tag{40}$$

With σ as our unit of length, we obtain

$$x=r/\sigma \tag{41}$$

and

$$\bar{n}^*=\bar{n}\sigma^3. \tag{42}$$

We introduce also the reduced temperature

$$T^*=kT/\epsilon. \tag{43}$$

The integral corresponding to the four-point double cross star was estimated by interpolating the results of Barker and Monaghan[22] and the other four-point stars were evaluated numerically for $T^*=2.74$. These results

[21] M. Klein, Phys. Fluids **7**, 391 (1963). The PY and CHNC isotherms are also taken from this paper.

[22] J. A. Barker and J. J. Monaghan, J. Chem. Phys. **36**, 2564 (1962).

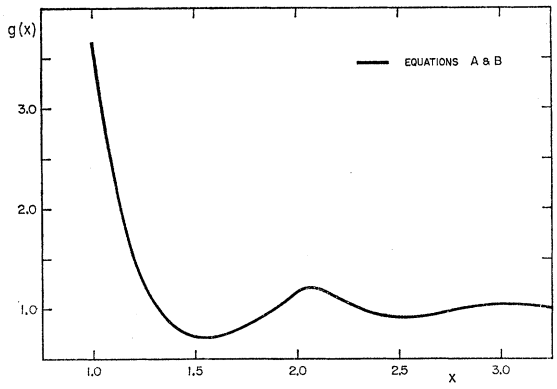

FIG. 13. Radial distribution functions for hard spheres for $\bar{n}^*=0.789$.

are listed in Fig. 9. Because solutions (MC, PY, and CHNC) have already been obtained for the $T^*=2.74$ isotherm for densities of $\bar{n}^*=0.40, 0.833, 1.00$, and 1.111, we chose to solve Eqs. (A) and (B) for these conditions. From Fig. 9 we obtain, for $T^*=2.74$,

$$m=-0.732 \tag{44}$$

and

$$a=0.0758. \tag{45}$$

Table I lists the values of m and a as a function of T^*

TABLE I. Values of the parameters m and a for the Lennard-Jones potential as a function of T^*.

T^*	m	a
20.0	−0.768	−0.025
8.0	−0.813	−0.128
4.0	−0.797	−0.053
2.0	−0.679	0.001
1.333	−0.634	−0.234
1.300	−0.626	−0.231
1.200	−0.589	−0.190

as determined from the Barker and Monaghan calculations. The radial distribution functions for $\bar{n}^*=0.40$,

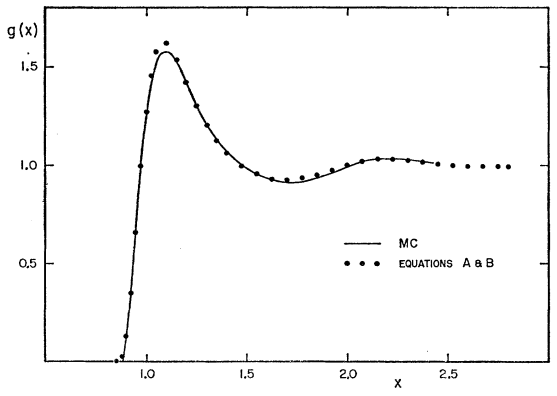

FIG. 14. Radial distribution functions for the Lennard-Jones potential for $T^*=2.74$ and $\bar{n}^*=0.40$.

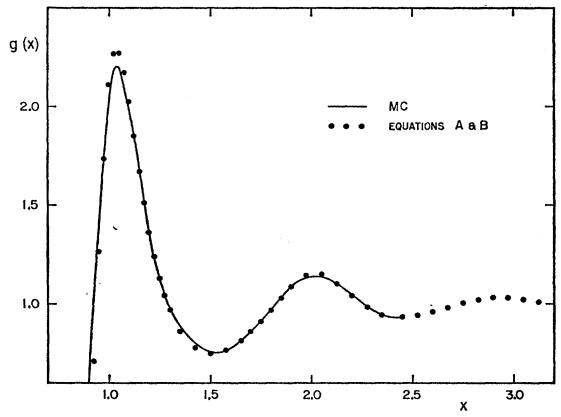

FIG. 15. Radial distribution functions for the Lennard-Jones potential for $T^*=2.74$ and $\bar{n}^*=0.833$.

TABLE II. Pressures and energies for the Lennard-Jones model for $T^*=2.74$.

	$\bar{n}^*=0.40$		$\bar{n}^*=0.833$		$\bar{n}^*=1.00$		$\bar{n}^*=1.111$	
	P^*	E	P^*	E	P^*	E	P^*	E
MC	1.2–1.5	−0.86	4.08	−1.57	6.97	−1.60	7.81	−1.86
(A)	1.24	−0.863	4.09	−1.56	6.99	−1.61	9.39	−1.54
(B)	1.24	−0.863	4.10	−1.58	6.99	−1.61	9.57	−1.51
CHNC	1.28	−0.859	5.11	−1.40	9.1	−1.19	13.2	−0.78
PY	1.24	−0.865	4.01	−1.61	6.8	−1.67	9.2	−1.59

0.833, and 1.00 are given in Figs. 14, 15, and 16 for MC, (A), and (B). Figure 17 shows the PY and CHNC results in addition to those listed above for $\bar{n}^*=1.111$. Table II lists the pressures (as determined by the pressure equation) and the energies.[23]

Once again the results from Eqs. (A) and (B) show much better agreement with MC than do the CHNC results, and the comparison with PY is very favorable.

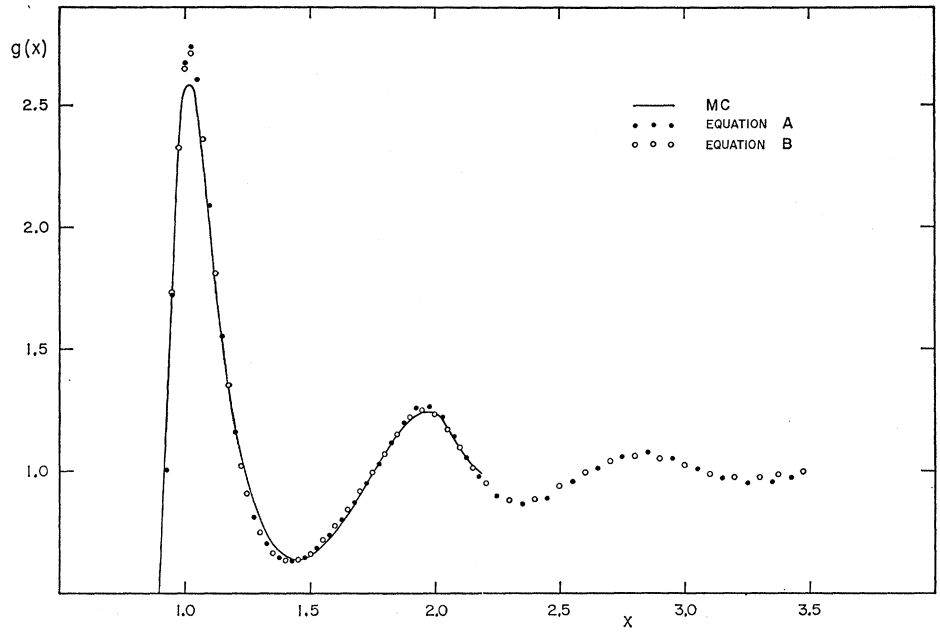

FIG. 16. Radial distribution functions for the Lennard-Jones potential for $T^*=2.74$ and $\bar{n}^*=1.00$.

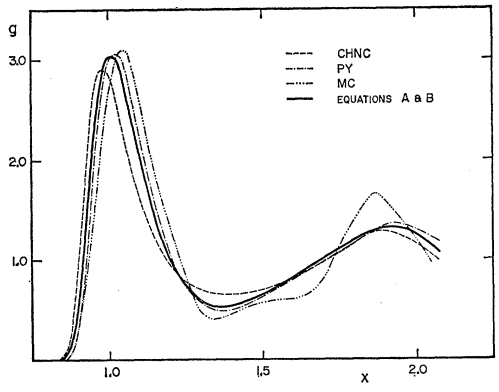

FIG. 17. Radial distribution functions for the Lennard-Jones potential for $T^*=2.74$ and $\bar{n}^*=1.111$.

V. CONCLUSION

Two integral equations have been proposed whose solutions yield approximations to the radial distribution functions of systems interacting with classical pairwise forces. The general form of these equations is such that good results are guaranteed for low densities. In addition

[23] The MC results are from Wood and Parker (Ref. 7) while the PY and CHNC results are from Broyles, Chung, and Sahlin (Ref. 4). Where there are several values of the thermodynamic quantities available in the MC method (because of different chain lengths and number of particles) we have chosen the value corresponding to the largest number of points in the chain per particle.

these equations each contain a parameter which may be chosen in an effort to improve the higher density solutions. For this paper we have chosen these parameters by examination of the early terms of the density series for $g\exp(\beta\phi)$ and the pressure. We have compared these new equations, with the MC method as the standard, against the PY and CHNC equations. These comparisons were made for the Gaussian, Lennard-Jones, and hard-sphere models. If we assume that MC is reasonably accurate, then we may conclude that the new equations show definite improvement over the CHNC equation in the hard-sphere and Lennard-Jones models, and improvement over PY for the Gaussian model, for the cases studied here. Because of small differences in the results and the uncertainty in the accuracy of all the solutions, it is not clear whether the new equations are any improvement over the PY equation in the hard-sphere and Lennard-Jones cases or the CHNC equation for the Gaussian cases.

At worst, we feel that the equations presented here will have the property of showing close agreement with either the PY or CHNC equations when one of them provides a good answer. We hope to be able to show definite improvement over both of these equations by selecting a case where neither the PY nor the CHNC equation provides an accurate answer. We feel that, relatively, in the case of the Lennard-Jones potential, the PY approximation should worsen and the CHNC approximation should improve as T^* is lowered.[24] If this is the situation there should exist a range in T^* where the new equations show definite improvement over both PY and CHNC. Also, a calculation at lower T^* should begin to show up the differences in Eqs. (A) and (B) and the differences in methods of choosing the parameters a and m. Unfortunately, it is unlikely that MC results are available in these regions and so a detailed study must await such a calculation.

The methods of choosing the parameters a and m used for this paper have the advantage of simplicity but are not necessarily the optimum. Further studies concerning the selection of a and m might lead to even better representations of the radial distribution functions over a wide range of temperatures, densities, and types of potentials.

ACKNOWLEDGMENTS

We wish to thank A. A. Broyles for several helpful suggestions during the course of this research and R. A. Smith for useful discussions concerning the numerical solutions of these equations. The computations were performed on the IBM-709 computer of the University of Florida Computing Center.

[24] See also Khan (Ref. 4) concerning this point.

PHYSICAL REVIEW VOLUME 137, NUMBER 1A 4 JANUARY 1965

Kompaneets Model for Radio Emission from a Nuclear Explosion

VICTOR GILINSKY
The RAND Corporation, Santa Monica, California
(Received 29 July 1964)

The electromagnetic signal from a nuclear explosion is computed using the same method as presented by Kompaneets. It is shown that some of Kompaneets' approximations are incorrect and lead to the wrong shape for the radiated signal. His work neglects the important first half-cycle of the signal and hence predicts an initial deflection in the wrong direction. A more accurate solution is presented.

I. INTRODUCTION

IN a 1958 article in the Soviet literature, Kompaneets[1] described the basic mechanism for radio emission from a nuclear explosion. This description, however, is incorrect at several points. The purpose of this paper is to show that a correct solution for the same model differs substantially from the solution presented by Kompaneets. In particular, he leaves out the important first half-cycle of the signal so that the initial deflection is in the wrong direction.

We shall use essentially the same method of calculation: We numerically integrate Maxwell's equations in dipole approximation, but with different conductivities and currents. We retain the electronic conductivity and neglect the ionic conductivity (he does the opposite) and we retain the Compton current in the field equations where he chooses to drop it (and therefore loses the first half-cycle).

[1] A. S. Kompaneets, Zh. Eksperim. i Teor. Fiz 35, 1538 (1958). [English transl.: Soviet Phys.—JETP 8, 1076 (1959)].

II. RADIATION MECHANISM

The radiation mechanism used by Kompaneets is essentially the following: A nuclear explosion emits a small fraction (say 0.1%) of its energy in the form of prompt gammas with a mean energy of one, or perhaps several, MeV. Kompaneets takes the time dependence

$$dN/dt=N_0be^{-bt} \tag{2.1}$$